Jurnal Teknologi

Full Paper

SYNTHESIS AND CHARACTERIZATION OF MAGNESIUM OXIDE-DOPED IRON (III) OXIDE NANOPARTICLES BY SOL-GEL METHOD

Haider J. Hassan[a*], Ahmed Y. Alam[b]

[a]University of Wasit, College of Education for Pure Sciences, Department of Physics, Wasit, Iraq
[b]University of Wasit, College of Science, Department of Physics, Wasit, Iraq

Article history
Received
6 July 2024
Received in revised form
13 January 2025
Accepted
13 January 2025
Published Online
22 August 2025

*Corresponding author
hjameel@uowasit.edu.iq

Graphical abstract

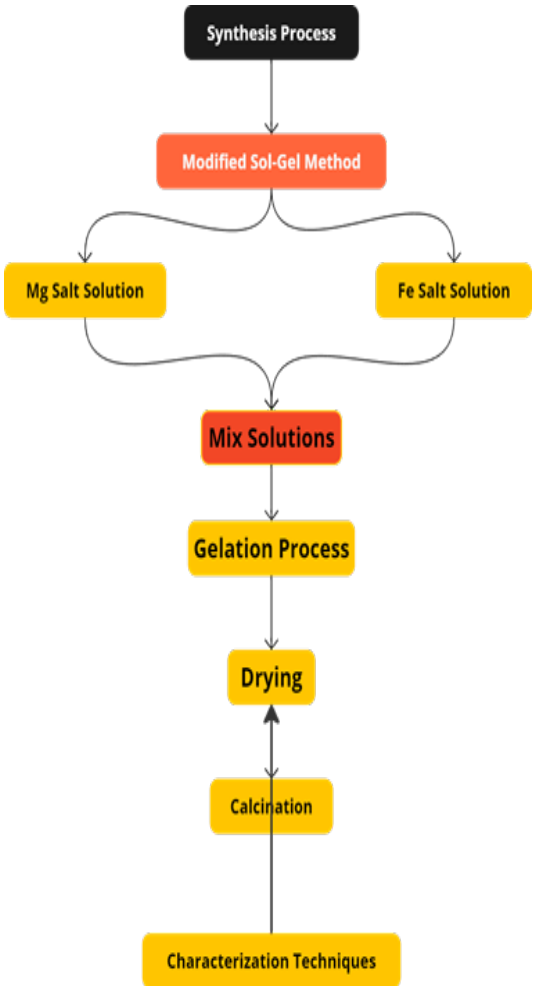

Abstract

This paper explores the synthesis and comprehensive characterization of magnesium oxide-doped iron (III) oxide nanoparticles (MgO-Fe_2O_3 NPs). Utilizing a modified sol-gel method, the study focused on integrating MgO and Fe_2O_3 to harness the synergistic effects of both metal oxides. The characterization techniques used include X-ray Diffraction (XRD), Fourier Transform Infrared Spectroscopy, UV-Vis spectroscopy, and Field Emission Scanning Electron Microscopy (FE-SEM), accompanied by Energy-dispersive X-ray Spectroscopy (EDX). Key findings from XRD analysis demonstrated a well-crystallized material with a range of crystallite sizes, calculated using the Scherrer formula, with an average size of 18.82 nm. FT-IR spectra identified several bonding interactions indicative of MgO and Fe_2O_3 phases, with specific peaks at 418, 549, and 1155 corresponding to metal-oxygen bonds and interactions. UV-V is absorbance measurements revealed a significant peak at 225 nm with a sharp decrease in absorbance at wavelengths above 300 nm, suggesting effective UV light absorption, which is critical for potential photocatalytic applications. The band gap estimated from Tauc plots was approximately 3 eV, confirming the material's suitability as a wide band gap semiconductor. The FE-SEM images indicated that the nanoparticles were spherical, with an average diameter of about 30 nm. This implies a uniform distribution and high surface area to volume ratio, which is indispensable for enhanced reactivity. EDX evidenced the composition of the nanoparticles, and the iron, magnesium, and oxygen peaks obviously doped the Fe_2O_3 into the MgO matrix. The synthesis of MgO-Fe_2O_3 nanoparticle sensors based on this novel sol-gel method opens an avenue to develop efficient sensors.

Keywords: Magnesium oxide nanoparticles, Iron oxide nanoparticles, FTIR, XRD, Magnesium Oxide-Doped Iron Oxide Nanoparticles

1.0 INTRODUCTION

Magnesium oxide (MgO) nanoparticles are highly attractive due to their strong ionic nature, simple crystal structure, well-defined stoichiometry, large specific surface area, and high density of reactive sites caused by numerous crystal defects [1, 2] Thus, this makes MgO nanoparticles an ideal material for a wide range of applications, including serving as antibacterial agents against foodborne pathogens, catalysts, ceramics, toxic waste remediation, paints, superconductor products, and adsorbents [3, 4] , In the recent years, several methods have been modified for the synthesis of MgO nanoparticles, such as solution combustion, micro-emulsion, chemical vapour deposition, laser ablation, pulsed laser deposition, microwave synthesis, hydrothermal, co-precipitation, solvothermal reduction, thermal decomposition, and sol-gel. Among them, the sol-gel technique is particularly favored due to its simplicity, high yield, low reaction temperatures, and ability to produce nanoparticles with a narrow size distribution and enhanced surface area. These characteristics are essential for improving reactivity and catalytic efficiency [5-7], The synthesis process usually involves complexing agents, such as magnesium acetate, in solvents like ethanol, oxalic acid, or tartaric acid. Upon annealing at high temperatures, these agents can introduce additional crystal defects, thereby increasing the number of active sites and modifying the surface properties of MgO Alongside advancements in MgO, iron oxide nanoparticles have gained significant attention due to their remarkable electronic, optical, magnetic, chemical, and thermal properties [8, 9], These properties make them suitable for a wide range of applications, including biotechnology, data storage, magnetic fluids, magnetic resonance imaging (MRI), environmental remediation, and catalysis [10, 11], Iron oxide, depending on its oxidation state, exists in various crystal structures, including hematite (a-Fe_2O_3), magnetite (γ-Fe_3O_4), and maghemite (c-Fe_2O_3). Hematite has attracted significant attention due to its wide range of applications, such as magnetic recording, catalysis, pigments, lithium-ion batteries, anticorrosive agents, gas sensors, water treatment, and photocatalysis [12, 13], Hematite is an environmentally friendly antiferromagnetic n-type semiconductor, and the most thermodynamically stable form of iron oxide at room temperature [14, 15]. The synthesis of a-Fe_2O_3 nanoparticles has been explored through various techniques, including magnetic sputtering, hydrothermal synthesis, sol-gel processes, ultrasonic spray pyrolysis, electrochemical anodization, and vapor-solid growth. These methods highlight the versatility and adaptability of iron oxide nanoparticles to different synthesis approaches [16]. This paper demonstrated to combine the advantages of both MgO and Fe_2O_3 by synthesizing MgO doped with Fe_2O_3 nanoparticles using a modified sol-gel method. The process incorporates citric acid and triethanolamine as gelling agents, selected for their cost-effectiveness, availability, and ability to form a homogeneous gel with iron (III) nitrate monohydrate. This approach enables the controlled production of metal-oxide nanoparticles that are chemically stable, uniformly sized, and well-dispersed [17, 18] , facilitating the controlled production of metal-oxide nanoparticles that are chemically stable, homogeneously sized, and well-dispersed [19-21]. more, it investigates the microstructure, morphology, bandgap, and photocatalytic properties of the MgO-Fe_2O_3 nanoparticles, with the potential to broaden their application in environmental and technological fields. Thus, we synthesized MgO-Fe_2O_3 nanoparticles using the sol-gel method and then calcined at 500°C for 3 hours. Also, the investigation included the determination of the average crystallite size, particle size distribution, and bandgap of these nanoparticles. [22, 23]. The current study employs a sol-gel process to examine the synthesis and characterization of MgO-Fe_2O_3 nanoparticle nanoparticles. This paper concerns themselves with their structural features and optical characteristics: integrity in spherical precipitate morphologies, average crystallite size of 18.82nm, and a band gap of 3eV that positions the MNPs for UV driven technologies and environmental cleanup efforts. On the other hand, this paper focuses on the work done by Kaur *et al*. (2020) on synthesising and characterising optically active Fe-doped MgO nanophosphors to explore their luminescence properties suitable for opto-electronic devices. According to Kaur, the increment of luminescence was found to be due to the Fe-doping of MgO and which altered the crystalline structure of the material. The current study improves the current knowledge of MgO-Fe_2O_3 systems assessing their potential for photocatalytic and catalytic application through UV absorption and active surface sites while Kaur *et al*. considered solely luminescent efficiencies for electronic purposes. Altogether, these works evidence the usefulness of MgO-based composites, while the present work can be considered as providing data on the application of the composites in environmental security, and Kaur's publication indicating the optoelectronics usability of the materials. The scope of the current work broadens the multi-functionality of use cases in technology and analytical environmental science [24].

2.0 METHODOLOGY

2.1 Materials and Equipment

- Magnesium nitrate hexahydrate [$Mg(NO_3)_2 \cdot 6H_2O$]
- Iron (III) nitrate nonahydrate [$Fe(NO_3)_3 \cdot 9H_2O$]
- Citric acid (as a chelating agent)
- Ethanol (solvent)
- Distilled water
- Magnetic stirrer with heating
- Oven for calcination
- Crucibles or ceramic dishes

2.2 MgO Doped with Fe_2O_3 Nanoparticle Synthesis

A 0.1 M solution of magnesium nitrate hexahydrate and a 0.05 M solution of iron (III) nitrate nonahydrate were dissolved in 100 mL of distilled water in a beaker. This molarity ratio was chosen to achieve a specific level of iron doping within the magnesium oxide matrix, although it could be adjusted based on the specific requirements of the study [25, 26]. Citric acid was then added to the solution in a 1:1 molar ratio relative to the total metal ion concentration, acting to stabilize the metal ions in the solution. To form the gel, ethanol was gradually introduced to the aqueous solution while continuously stirring to ensure uniform mixing [27, 28]. The volume of ethanol added was equal to the volume of the aqueous solution. The mixture was then heated to 80°C on a magnetic stirrer and maintained at this temperature for 2 hours to facilitate complete sol formation. During this stage, citric acid functioned as a chelating agent, complexing with the metal ions and contributing to the gelation process [29, 30]. After sol formation, the solution was cooled to room temperature and allowed to age for 24 hours under calm conditions, a crucial step for promoting further polymerization and strengthening the gel network. The gel was then dried in an oven at 120°C for 12 hours to remove residual solvents and water, resulting in an aerogel [31]. The dry gel was calcined in a crucible at 500°C for 3 hours to decompose organic materials and facilitate the formation of magnesium oxide (MgO) and iron oxide (Fe_2O_3) in their respective phases. The high temperature promoted the formation of both MgO and Fe_2O_3 while also aiding in the creation of a porous structure.

3.0 RESULTS AND DISCUSSION

3.1 FT-IR Analysis

The obtained FT-IR spectrum shows distinct peaks at various frequencies, each corresponding to specific functional groups and bonding interactions within the MgO/Fe_2O_3 nanoparticles. A schematic analysis of the spectrum based on the observed peaks is provided in Figure 1. The FT-IR spectrum of the MgO/Fe_2O_3 nanoparticles reveals several characteristic peaks that offer insights into its structural and chemical properties.The peak at 418 cm^{-1} corresponds to Fe-O stretching vibrations in Fe_2O_3, indicating the presence of metal-oxygen bonds in the iron oxide phase [32]. Another peak at 549 cm^{-1} suggests variations in Fe-O stretching, which may be due to different interactions between Fe_2O_3 and MgO, potentially reflecting their structural integration [33]. The peak at 1155 cm^{-1} is likely attributed to Mg-O stretching vibrations, confirming the presence of MgO and indicating some degree of interaction with Fe_2O_3 [34].

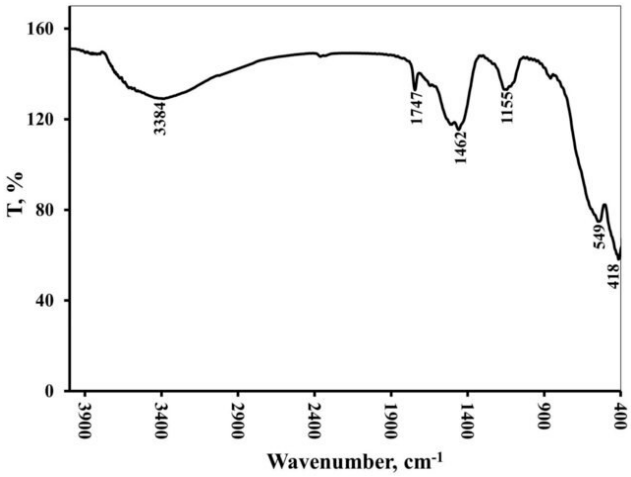

Figure 1 FT-IR spectrum of the prepared MgO/Fe_2O_3 nanocomposite

3.2 XRD Analysis

Figure 2 shows the XRD diffraction pattern of a MgO compound doped with Fe_2O_3, providing insights into its crystalline structure and particle size. The XRD data reveals a major peak corresponding to a prominent crystallographic plane, which is Indicative of a well-defined crystalline structure. Peaks at 111, 311, 200, and 313 further confirm the presence of distinct crystal phases of both MgO and Fe_2O_3, suggesting that the material is well-crystallized [39]. To calculate the crystallite sizes, the Scherrer formula is used, which relates the width of the diffraction peaks (the Full Width at Half Maximum) to the size of the coherent diffracting domains, or crystallites. The Scherrer equation is typically expressed as [40]:

$$D = k\lambda\beta\cos\theta$$

where:
D is the crystallite size,
K is the shape factor (often taken as 0.9),
λ is the X-ray wavelength,
β is the FWHM of the peak.
θ is the Bragg angle (half of the 2θ)

Based on the XRD data, the crystallite sizes of the MgO/Fe_2O_3 nanoparticles vary significantly, with values of 42.83 nm, 41.08 nm, 0.57 nm, 8.50 nm, 14.58 nm, and 5.37 nm. This variation suggests a distribution of crystallite sizes within the sample, which could influence properties such as reactivity, stability, and overall performance. The calculated average crystallite size of 18.82 nm represents the typical domain size of the coherent crystalline regions throughout the sample. The XRD peaks observed at 29.36541°, 38.94883°, 32.10017°, 42.73727°, 47.97°, and 62.27° correspond well with the identified hkl planes, providing essential information for phase identification and confirming the crystalline nature of the sample [39]. The specific indices for these phases, Fe_2O_3 (96-

153-9748) and MgO (96-100-0054), are in line with standard crystallographic data entries for these materials, validating the presence of both MgO and Fe_2O_3 phases in the nanoparticles. This finding is consistent with the work of Anjali Gupta *et al.*, further confirming the crystalline nature and phase composition of the synthesized MgO/Fe_2O_3 nanoparticles[41].

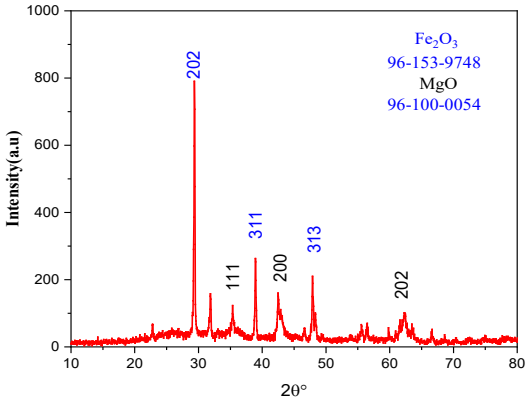

Figure 2 XRD patterns of the MgO/Fe_2O_3 nanocomposite

3.3 UV-Visible Analysis

Figure 3 shows The UV-Vis absorption spectrum of the MgO/Fe_2O_3 nanocomposite synthesized at 500°C shows intense optical features where the high absorption coefficient in the UV region (200–300 nm) could be ascribed to the CT transitions between oxygen ions (O^{2-}) and metal cations (Fe^{3+} or Mg^{2+}). This absorption implies a wide band gap typical of semiconducting oxides, which should point toward usage of the material in applications involving UV interaction including photocatalytic and environmental uses. There is also an abrupt decline of absorption after 300 nm which is further consistent with the limited visible light absorption inherent to the composite. The substrate annealing at high temperature might also increase the material's crystallinity and minimize defect conditions as described by the sharp absorption edge which can be ideal for UV driven processes and other procedures that demand steady optical and catalytic property.

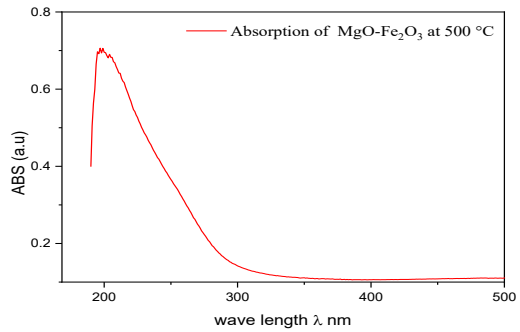

Figure 3 Absorbance spectrum of MgO/Fe_2O_3

Evaluation of the absorbance curve, particularly the sharp and intensive peak in the UV region with the following sharp decrease is characteristic of nanoscale materials which, because of developing quantum confinement effects and a high SSA, have peculiar optical properties. The high temperature synthesis at 500°C may improve the crystallinity and decrease the defect states which may possibly explain the sharper absorption edge and better optical characteristic. In addition, the doped iron oxide in the composite assumes a role in the electronic character and affinity of the composite with magnesium oxide for UV light absorption. These alternative properties make the MgO/Fe_2O_3 nanocomposite very appropriate for UV driven applications using its nanoscale formation and photo activity this is in agreement with Srivastava *et al.* [42]. Figure 4 shows the Tauc plot, which is typically used to determine the optical band gap of semiconductor materials. In this plot, the $(\alpha h\nu)^2$ is plotted against the photon energy, where a is the absorption coefficient and hν is the photon energy. The graph represents the band gap analysis for a magnesium oxide (MgO) compound doped with iron oxide (Fe_2O_3).

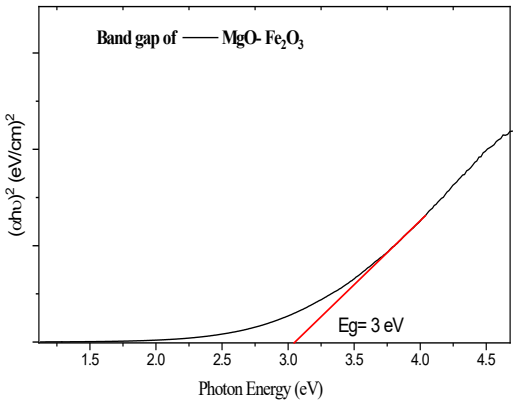

Figure 4 Tauc plot the MgO- Fe_2O_3 Band gap

A band gap of 3 eV indicates that the material absorbs ultraviolet light but not visible light [43], which typically starts at around 1.65 eV (750 nm) and extends to about 3.1 eV (400 nm). This aligns with the UV absorbance spectrum shown previously, which showed strong absorption in the UV region and minimal in the visible range. Semiconductor Type The band gap value categorizes this material as a wide band gap semiconductor, making it suitable for applications where resistance to electrical conductivity in the visible light spectrum is desired, and efficiency in UV light absorption is beneficial. Photocatalytic and Electronic Applications: Materials with a band gap of around 3 eV are commonly used in photocatalysts and electronic devices that operate under UV light. The ability to absorb high-energy photons and then utilize the generated electron-hole

pairs can be applied in photocatalysis (e.g., breaking down pollutants or water splitting to generate hydrogen). The influence of Doping, Doping MgO with Fe_2O_3 could be altering the electronic structure, resulting in the modification of the band gap. Iron oxide itself has different polymorphs with varying band gaps, and its integration into MgO might provide a means to tune the band gap to the observed value [44]. Smith *et al*. (2022) have also pointed out that UV-visible spectroscopy for Fe2O3 – doped ZnO shows a major shift towards red when compared to ZnO.Presenting in this red shift, Fe_2O_3 demonstrates that it can improve the band gap through mid-gap defect states for the uptake of visible-light.red to pure ZnO. This red shift indicates that Fe_2O_3 effectively narrows the band gap by introducing mid-gap defect states, enhancing visible-light absorption. This kind of band-gap tuning is especially relevant to enhance the photocatalytic performances under solar light conditions; it opens a new pathway for further photocatalytic work in environmental clean-up processes[45]. Based on the study by Lee and Park (2023), the incorporation of Fe2O3 in ZnO creates a considerable slope in the visible area, which may induce a different optical absorption compared with the native one of the undoped ZnO. Interaction of Fe_2O_3 ions and ZnO lattice may lower electron-hole recombination rates as shown by the decrease in photoluminescence intensity suggesting that Fe_2O_3 doped ZnO holds as a potential candidate for improved photoelectrochemical and sensing applications [46].

3.4 FE-SEM (Field Emission Scanning Electron Microscopy

Figure 5 shows the magnesium oxide (MgO) doped with iron oxide (Fe_2O_3), including the morphology (shape and size), the distribution, and specific surface features of the nanoparticles.

The reported size is approximately 30 nm. This size falls within the nano-regime, which can significantly influence the material's properties, including increased reactivity and quantum mechanical effects. Spherical nanoparticles are often desired for certain applications due to their symmetry and high surface area to volume ratio. Spherical shapes in nanoparticle synthesis can suggest a uniform growth mechanism during the synthesis process A good distribution of particles, where the spherical shapes are evenly spread over the entire scanned area, suggests a well-controlled synthesis process. Uniform distribution helps in achieving consistent properties across the bulk material. any areas where particles seem to cluster together. Agglomeration shown in Figure 5 can affect the effective surface area and, hence, the reactivity of nanoparticles. In applications such as catalysis, reduced agglomeration is often beneficial. Check for the smoothness or roughness of the individual nanoparticles. Surface irregularities can influence how nanoparticles interact with their environment.

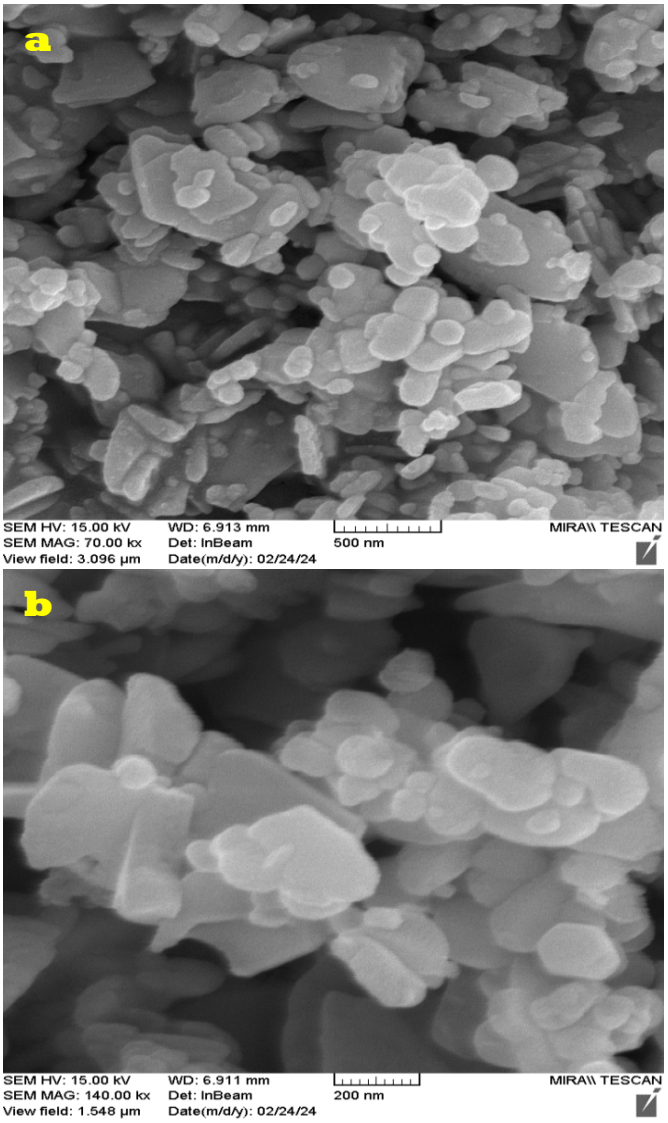

Figure 1 (a) Structural representation of magnesium oxide (MgO) doped with iron oxide (Fe_2O_3), illustrating material composition and interactions (b) High-magnification image for (MgO-Fe_2O_3)

The presence of pores or voids can also be relevant, especially in catalytic applications, as they can facilitate the diffusion of reactants to the active sites. ensure there is a scale bar to validate the size estimation of 30 nm. The scale bar is crucial for confirming that the nanoparticles meet the described size. The resolution of the image should be high enough to clearly resolve individual particles and not just clusters. These should be adjusted to clearly distinguish nanoparticles from the background, allowing for accurate analysis of distribution and morphology

3.5 Energy-dispersive X-ray Spectroscopy

Energy-dispersive X-ray Spectroscopy (EDX or EDS) analysis, is commonly used in conjunction with scanning electron microscopy (SEM) to determine the

elemental composition of a sample. The spectrum in Figure 6 shows peaks corresponding to the elements oxygen (O), iron (Fe), and magnesium (Mg), which are constituents magnesium oxide (MgO) doped with iron oxide (Fe_2O_3).

Each peak in the EDX spectrum corresponds to a characteristic X-ray emitted by an element when it is struck by the electron beam in the SEM. The energy of these X-rays is specific to the electron transitions within the atoms of each element. The tall and sharp peaks at the lower energy side of the spectrum (around 0.5 keV) indicate a high content of oxygen. This is expected as both MgO and Fe_2O_3 are oxides. The peaks for magnesium are visible around 1.25 keV, characteristic of Mg's K-series X-ray emissions. There are significant peaks for iron, especially around 6.4 keV, which belong to Fe's K-series. This confirms the presence of iron oxide as a dopant. The quantitative data for oxygen (78.86% atomic percent, 2.01% weight percent) suggests that oxygen is the most abundant element by atomic ratio, which is typical for oxide compounds. Iron makes up 6.84% atomic percent and 0.16% weight percent of the sample. This indicates a substantial incorporation of Fe in the material, likely as Fe_2O_3. Magnesium constitutes 14.30% atomic percent and 0.25% weight percent, indicating that Mg is the primary metal component, forming the base matrix of MgO [47].

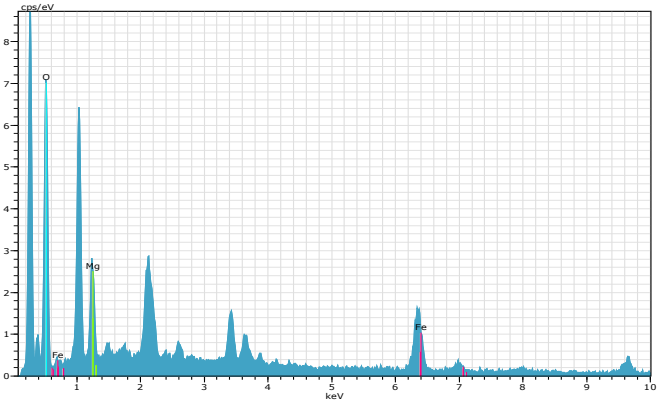

Figure 6 Energy-dispersive X-ray Spectroscopy (EDX to the elements oxygen (O), iron (Fe), and magnesium (Mg))

4.0 CONCLUSION

This study successfully synthesized magnesium oxide-doped iron (III) oxide nanoparticles (MgO-Fe_2O_3 NPs) using a modified sol-gel process, an innovative approach aimed at enhancing the material's properties. Detailed characterization through X-ray diffraction (XRD) and Fourier-transform infrared (FTIR) spectroscopy confirmed the formation of a cubic crystal structure and the presence of characteristic bonding, validating the successful doping of MgO with Fe_2O_3. Further analysis using field emission scanning electron microscopy (FESEM) revealed the development of spherical nanoparticles with a uniform size distribution, which is crucial for optimizing the material's reactive surface area. Optical characterization via diffuse reflectance spectroscopy and the analysis of the UV absorbance spectrum provided insights into the material's electronic properties, particularly its high energy band gap, which is advantageous for UV shielding and potential photocatalytic applications. Energy-dispersive X-ray spectroscopy (EDX) further confirmed the integration of iron into the MgO matrix, reinforcing the effectiveness of the doping process. The combination of the material's environmental stability and favorable electronic properties positions MgO-Fe_2O_3 nanoparticles as highly promising candidates for use in environmental monitoring and remediation applications. The results of this study suggest that the synthesis method, aligned with current technological advancements and environmental safety considerations, provides a strong foundation for potential real-world applications. Further research is needed to assess the scalability and long-term stability of these nanoparticles under various environmental conditions, which would be essential for their commercialization in applications such as gas sensors and other important technologies.

Acknowledgement

This research is fully supported by the authors The authors fully acknowledged the Iraqi Ministry of Higher Education and Scientific Research, University of Wasit, College of Education for Pure Science, Department of Physics, Wasit, Iraq which makes this important research viable and effective.

Conflicts of Interest

The authors declare that there is no conflict of interest regarding the publication of this paper.

References

[1] T. Jeena, M. Geetha, P. Suchetan, N. Ronald, and K. Amrutha. 2023. Influence of Cobalt Doping on Chemical and Green Synthesized Magnesium Oxide Nanoparticles for Enhanced Photocatalytic Evaluation, Adsorption Studies, Antimicrobial Analysis and Corrosion Inhibition Study. *Inorganic Chemistry Communications*. 157: 111232.

[2] N. M. Julkapli and S. Bagheri. 2016. Magnesium Oxide as a Heterogeneous Catalyst Support. *Reviews in Inorganic Chemistry*. 36(1): 1–41.

[3] A. A. Pilarska, Ł. Klapiszewski, and T. Jesionowski. 2017. Recent Development in the Synthesis, Modification and Application of Mg $(OH)_2$ and MgO: A Review. *Powder Technology*. 319: 373–407.

[4] T. Jeena, M. P. Geetha, P.A. Suchetan, N. Ronald, K. Amrutha. 2023. Influence of Cobalt Doping on Chemical and Green Synthesized Magnesium Oxide Nanoparticles for Enhanced Photocatalytic Evaluation, Adsorption Studies, Antimicrobial Analysis and Corrosion Inhibition Study. *Inorganic Chemistry Communications*. 157.

[5] F. Bensebaa, 2012. Nanoparticle Technologies: Chapter 2. Wet Production Methods. Elsevier Inc.

[6] I. Bretos *et al.* 2020. Low-temperature Solution Crystallization of Nanostructured Oxides and Thin Films. *Chemistry–A European Journal.* 26(42): 9157–9179.
[7] Z. Vaseghi and A. Nematollahzadeh. 2020. Nanomaterials: Types, Synthesis, and Characterization. *Green Synthesis of Nanomaterials for Bioenergy Applications.* 23–82.
[8] N. F. Raduwan, N. Shaari, S. K. Kamarudin, M. S. Masdar, and R. M. Yunus. 2023. Structural Transformation Doubly Triggered by Hydrothermal Temperature and Reaction Time in 3D Mixed Transition Metal Oxide: Great Enhancement of Pore Size Distribution and Specific Surface Area. *International Journal of Hydrogen Energy.* 48(70): 27289–27297.
[9] P. G. Jamkhande, N. W. Ghule, A. H. Bamer, and M. G. Kalaskar. 2019. Metal Nanoparticles Synthesis: An Overview on Methods of Preparation, Advantages and Disadvantages, and Applications. *Journal of Drug Delivery Science and Technology.* 53: 101174.
[10] N. Ajinkya, X. Yu, P. Kaithal, H. Luo, P. Somani, and S. Ramakrishna. 2020. Magnetic Iron Oxide Nanoparticle (IONP) Synthesis to Applications: Present and Future. *Materials.* 13(20): 4644.
[11] S. S. Laha *et al.* 2022. Rare-earth Doped Iron Oxide Nanostructures for Cancer Theranostics: Magnetic Hyperthermia and Magnetic Resonance Imaging. *Small.* 18(11): 2104855.
[12] J. E. Ogbezode, U. S. Ezealigo, A. Bello, V. C. Anye, and A. P. Onwualu. 2023. A Narrative Review of the Synthesis, Characterization, and Applications of Iron Oxide Nanoparticles. *Discover Nano.* 18: 125.
[13] S. Sen and K. Sarkar. 2017. Heavy Metal Remediation Potential of Metallic Nanomaterials Synthesized by Microbes. *Handbook of Metal-Microbe Interactions and Bioremediation*. CRC Press. 401–420.
[14] P. Nam Hai *et al.* 2012. Growth and Characterization of n-type Electron-induced Ferromagnetic Semiconductor (In, Fe) As. *Applied Physics Letters.* 101(18).
[15] B. Mekuye, D. Atnafu, A. Yibeltal, and M. Abera. 2024. Computational Investigation of High Curie Temperature in a New N-type Ferromagnetic Diluted Magnetic Semiconductors, Especially Iron-doped on GaSb. *Nano Select.* e2300194.
[16] S. Zhuiykov. 2018. *Nanostructured Semiconductors*. Woodhead Publishing.
[17] S. Kumar and X. T. Cao. 2024. Natural Bio-sourced Polymers: Emerging Precursors for the Synthesis of Single Atom Catalysts. *Coordination Chemistry Reviews.* 499: 215524.
[18] M. Askarieh, H. Farshidi, A. Rashidi, A. Pourreza, and M. S. Alivand. 2022. Comparative Evaluation of MIL-101 (Cr)/calcium Alginate Composite Beads as Potential Adsorbents for Removing Water Vapor from Air. *Separation and Purification Technology*. 291: 120830.
[19] S. Wang *et al.* 2023. Surface Functionalization of Metal and Metal Oxide Nanoparticles for Dispersion and Tribological Applications-A Review. *Journal of Molecular Liquids.* 122821.
[20] C. Ding *et al.* 2019. Abundant Hydrogen Production Over Well Dispersed Nickel Nanoparticles Confined in Mesoporous Metal Oxides in Partial Oxidation of Methane. *International Journal of Hydrogen Energy.* 44(57): 30171–30184.
[21] Z. B. Shifrina, V. G. Matveeva, and L. M. Bronstein. 2019. Role of Polymer Structures in Catalysis by Transition Metal and Metal Oxide Nanoparticle Composites. *Chemical Reviews.* 120(2): 1350–1396.
[22] V. V. Mitić, N. Obradović, and L. Mančić. 2013. Advanced Ceramics and Application: New Frontiers in Multifunctional Material Science and Processing: Program and the Book of Abstracts: II Serbian Ceramic Society Conference, Sep 30th-Oct 1st, 2013, Belgrade. Belgrade: Serbian Ceramic Society.
[23] T. Čtvrtníčková. 2008. Analysis of Solid Materials by Means of Laser-induced Breakdown Spectroscopy. Doctoral Thesis. Masaryk University, Faculty of Science, Brno.
[24] P. Kaur, A. Kaur, S. Singh, S. Thakur, and L. Singh. 2020. Comprehensive Analysis of Crystal Structure, Optical and Luminescent Behavior of Fe Doped MgO Nanophosphors. *Optik.* 219: 164742.
[25] B. B. Qassim and H. J. Abdullah. 2022. Sensitive Spectrophotometric Estimation of Thiol Drugs (Mesna) in Pure, Pharmaceutics and Serum Samples via a New Method of FI System using Iron (III) Nitrate Nonahydrate as Oxidizing Agent. *International Journal of Mechanical Engineering.*
[26] M. Mantovani, E. Collina, M. Lasagni, F. Marazzi, and V. Mezzanotte. 2023. Production of Microalgal-based Carbon Encapsulated Iron Nanoparticles (ME-nFe) to Remove Heavy Metals in Wastewater. *Environmental Science and Pollution Research.* 30(3): 6730–6745.
[27] T. B. da Costa, M. G. C. da Silva, and M. G. A. Vieira. 2021. Development of a Natural Polymeric Bioadsorbent based on Sericin, Alginate and Poly (vinyl alcohol) for the Recovery of Ytterbium from Aqueous Solutions. *Journal of Cleaner Production.* 279: 123555.
[28] X. Zhang, M. Feng, R. Qu, H. Liu, L. Wang, and Z. Wang. 2016. Catalytic Degradation of Diethyl Phthalate in Aqueous Solution by Persulfate Activated with Nano-scaled Magnetic $CuFe_2O_4$/MWCNTs. *Chemical Engineering Journal.* 301: 1–11.
[29] I. D. Sideridou and M. M. Karabela. 2011. Sorption of Water, Ethanol or Ethanol/water Solutions by Light-cured Dental Dimethacrylate resins. *Dental Materials.* 27(10): 1003–1010.
[30] V. Y. Gotsul'skii, N. Malomuzh, and V. Chechko. 2013. Features of the Temperature and Concentration Dependences of the Contraction of Aqueous Solutions of Ethanol. *Russian Journal of Physical Chemistry A.* 87: 1638–1644.
[31] B. Yu *et al.* 2012. Effect of Calcium Source on Structure and Properties of Sol–gel Derived Bioactive Glasses. *Langmuir.* 28(50): 17465-17476.
[32] Y. Yue *et al.* 2024. Catalytic Conversion of Ethyl Levulinate to γ-Valerolactone Under Mild Conditions over Zr-Beta Acidic Zeolite Prepared by Hydrothermal Method. *Catalysts.* 14(12): 924.
[33] S. J. Jayaseelan, K. Parasuraman, D. B. Anburaj, M. Jothibas, and B. Arunkumar. 2023. The Impacts of Mn Ion Incorporation on the Structural, Optical, and Magnetic Properties of Hematite NPs. *Nanotechnology for Environmental Engineering.* 8(1): 15–26.
[34] F. O. Michael, O. J. Olalekan, A. C. Uzorna, and A. A. Seember. 2024. Improving Cowpea (Vigna unguiculata (L.) Walp.) Yield with Green Synthesized Mgo Nanoparticles Using Jatropha Tajonensis Leaf Extract. *Biotechnologia Acta.* 17(4): 60–74.
[35] W. Li, Y. Huang, T. Wang, M. Fang, and Y. Li. 2022. Preparation of Calcium Carbonate Nanoparticles from Waste Carbide Slag based on CO_2 Mineralization. *Journal of Cleaner Production.* 363: 132463.
[36] R. Khan, M. A. Inam, D. R. Park, S. Khan, M. Akram, and I. T. Yeom. 2019. The Removal of CuO Nanoparticles from Water by Conventional Treatment C/F/S: The Effect of pH and Natural Organic Matter. *Molecules.* 24(5): 914.
[37] M. Kassaee, E. Motamedi, and M. Majdi. 2011. Magnetic Fe_3O_4-graphene Oxide/polystyrene: Fabrication and Characterization of a Promising Nanocomposite. *Chemical Engineering Journal.* 172(1): 540–549.
[38] E. Fritsch, E. Balan, S. Petit, and F. Juillot. 2021. Structural, Textural, and Chemical Controls on the OH Stretching Vibrations in Serpentine-group Minerals. *European Journal of Mineralogy.* 33(4): 447–462.
[39] Z. M. Alaizeri, H. A. Alhadlaq, S. Aldawood, and M. Ahamed. 2024. Synthesis and Characterization of MgO-Fe_2O_3/γ-Al_2O_3 Nanocomposites: Enhanced Photocatalytic Efficiency and Selective Anticancer Properties. *Catalysts.* 14(12): 923.
[40] C. Hu *et al.* 2024. Insights into the Role of Pt Promoter in Co/TiO_2 Catalysts for CO Hydrogenation. *Catalysts.* 14(12): 922.

[41] Anjali *et al.* 2024. Enhancing Photocatalytic Performance of Fe_3O_4 Nanoparticles and Fe_3O_4@ ZnO Nanocomposites. *Ionics*. 1–13.
[42] M. K. Srivastava, V. Agarwal, H. Kumari, S. Sharma, R. Kumar, and S. Chahal, "Synthesis, Characterization, and Enhanced Photocatalytic Degradation of Rose Bengal (RB) Dye Using an a-Fe2O3/MgO Nanocomposite," *Journal of Electronic Materials,* pp. 1-12, 2024.
[43] J. Xie, Z. Zhou, Y. Lian, Y. Hao, P. Li, and Y. Wei. 2015. Synthesis of a-Fe_2O_3/ZnO Composites for Photocatalytic Degradation of Pentachlorophenol under UV–vis Light Irradiation. *Ceramics International.* 41(2): 2622–2625.
[44] E. Kamali, F. Dreekvandy, A. Mohammadkhani, and A. Heydari. 2024. Modified Nano Magnetic Fe_2O_3-MgO as a High Active Multifunctional Heterogeneous Catalyst for Environmentally Beneficial Carbon–carbon Synthesis. *BMC Chemistry*. 18(1): 78.
[45] D. A. Smith, Johnson, M. K., & Alvarez, S. C. 2022. Enhanced Visible-light Absorption in Fe-doped ZnO Nanostructures and Its Impact on Photocatalytic Performance. *Materials Science in Semiconductor Processing.* 136: 106170.
[46] J. H. Lee, & Park, S. Y. 2023, Fe-$_2O_3$ -engineered ZnO Photoanodes with Reduced Recombination and Improved Solar-driven Water Splitting. *Applied Surface Science.* 613: 156049.
[47] H. Sridevi, M. R. Bhat, P. S. Kumar, N. M. Kumar, and R. Selvaraj. 2023. Structural Characterization of Cuboidal a-Fe_2O_3 Nanoparticles Synthesized by a Facile Approach. *Applied Nanoscience.* 13(8): 5605–5613.